

Article

# Experimental Investigations Conducted for the Characteristic Study of OM29 Phase Change Material and Its Incorporation in Photovoltaic Panel

Rajvikram Madurai Elavarasan <sup>1,\*</sup>, Karthikeyan Velmurugan <sup>2,3,\*</sup>, Umashankar Subramaniam <sup>4</sup> ,  
A Rakesh Kumar <sup>5</sup>  and Dhafer Almahles <sup>4</sup> 

<sup>1</sup> Department of Electrical and Electronics Engineering, Sri Venkateswara College of Engineering, Chennai, 602117 Tamil Nadu, India

<sup>2</sup> School of Renewable Energy and Smart Grid Technology, Naresuan University, 65000 Phitsanulok, Thailand

<sup>3</sup> Center for Alternative Energy Research and Development, Khon Kaen University, 40002 Khon Kaen, Thailand

<sup>4</sup> Renewable Energy Laboratory, Faculty of Engineering, Prince Sultan University, 11586 Riyadh, Saudi Arabia; shankarums@gmail.com (U.S.); dalmakhles@psu.edu.sa (D.A.)

<sup>5</sup> Department of Electrical and Electronics Engineering, National Institute of Technology, 620015 Tiruchirappalli, India; rakesh.a@ieee.org

\* Correspondence: rajvikram787@gmail.com (R.M.E.); karthi230407@gmail.com (K.V.)

Received: 17 January 2020; Accepted: 12 February 2020; Published: 18 February 2020



**Abstract:** The solar photovoltaic (PV) system is emerging energetically in meeting the present energy demands. A rise in PV module temperature reduces the electrical efficiency, which fails to meet the expected energy demand. The main objective of this research was to study the nature of OM29, which is an organic phase change material (PCM) used for PV module cooling during the summer season. A heat transfer network was developed to minimize the experimental difficulties and represent the working model as an electrical resistance circuit. Most existing PV module temperature ( $T_{PV}$ ) reduction technology fails to achieve the effective heat transfer from the PV module to PCM because there is an intermediate layer between the PV module and PCM. In this proposed method, liquid PCM is filled directly on the back surface of the PV module to overcome the conduction barrier and PCM attains the thermal energy directly from the PV module. Further, the rear side of the PCM is enclosed by tin combined with aluminium to avoid any leakages during phase change. Experimental results show that the PV module temperature decreased by a maximum of 1.2 °C using OM29 until 08:30. However, after 09:00, the OM29 PCM was unable to lower the  $T_{PV}$  because OM29 is not capable of maintaining the latent heat property for a longer time and total amount of the PCM experimented in this study was not sufficient to store the PV module generated thermal energy for an entire day. The inability of the presented PCM to lower the temperature of the PV panel was attributed to the lower melting point of OM29. PCM back sheet was incapable of dissipating the stored PCM's thermal energy to the ambient, and this makes the experimented PCM unsuitable for the selected location during summer.

**Keywords:** Organic PCM; PV module cooling; Thermal absorption; Thermal dissipation

## 1. Introduction

The global energy demand has increased by 2.3% compared to 2010, and this increase is mainly due to modernization and industrialization [1]. Air pollution has increased significantly because of the forest to agricultural land transformation, burning of fossil fuels, dumping waste into water, burning waste, and vehicle smoke emission. This increases by 1.7% the CO<sub>2</sub> concentration every year, leading to

a threatening global climate change [2–4]. To overcome this issue, renewable energy systems are widely engaged to meet energy demand [5]. Among other renewable energy sources, solar photovoltaic (PV) systems gain attention for their low maintenance and payback period. A great amount of research work is also carried out on PV materials to improve the efficiency of PV panel [6,7]. The PV system can be operated on a standalone basis or in grid connected mode [8–12]. Crystalline silicon solar cell converts 1/5th of the photon into electrical energy, while some is reflected, and this reflection can be controlled by coating a thin layer of  $\text{Al}_2\text{O}_3$  and  $\text{Ta}_2\text{O}_5$  [13], and the rest is almost converted into thermal energy. Excess thermal energy in the PV module results in the drop of efficiency by 0.3–0.4% for every 1 °C more than the nominal operating cell temperature [14]. Further reduction in  $T_{\text{PV}}$  can increase the performance of the system.

Earlier PV module cooling was conducted using water or air as a cooling agent. Water has a high specific heat capacity (4.2 J/g·K), and it can absorb higher thermal energy from the PV module. Water-assisted PV modules are mostly performed as an active method by spraying water over the PV module [15] or using heat pipe behind the PV module for both the electrical and thermal applications [16,17]. Other than active method, thermosiphon concept has also been tested but the result lowers the  $T_{\text{PV}}$  reduction [18]. Air-based PV module cooling is mostly examined for hybrid applications where hot air is used for thermal comfort and space heating [19,20]. In most cases, water and air-based  $T_{\text{PV}}$  reductions are not convenient due to lack of resource.

In recent years, phase change material (PCM)-assisted PV module cooling has gained great attention in terms of its striking latent heat of fusion [21,22]. PCM can extract the generated thermal energy from the PV module, and it is stored in the form of specific heat capacity and latent heat of fusion; this is as expressed in Equation (1) [23]. PCM-aided PV modules are prominent and they depend on the application of cooling methods chosen, either active or passive.

$$Q = \int_{T_i}^{T_m} mC_{p,s}dT + mL + \int_{T_m}^{T_e} mC_{p,l}dT \quad (1)$$

where  $T_i$  is initial temperature,  $T_m$  is melting temperature,  $T_e$  is ending temperature,  $m$  is total mass of PCM,  $C_{p,s}$  is solid specific heat capacity of PCM,  $C_{p,l}$  is liquid specific heat capacity of PCM,  $L$  is latent heat capacity of the PCM, and  $Q$  is the total amount of energy stored in the PCM.

Active cooling methods are implemented for the performance enhancement of electrical and thermal energy using working fluids [24,25]. This active method requires less PCM because it is assisted with working fluid and periodically PCM temperature is removed by working fluid, which enables the heat transfer between the PV module and PCM. Fayaz et al. performed COMSOL simulation for a photovoltaic–thermal (PVT) system with and without PCM using heat exchanger-assisted model and compared it with the PV module [26]. They found that numerical simulation results are accurate compared to the experimental result and the remarkable increase in flow rate leads to reduce the  $T_{\text{PV}}$  maximum by 13.77 °C. Al-Waeli et al. studied a nano PCM and nanofluid-assisted PVT collector, a copper absorber tube entrenched with nano PCM, to extract the heat from PCM container by flowing nanofluid, which enhances the thermal energy transfer from PV to PCM container [27]. Silicon oil is placed between the PV module rear surfaces and the PCM container to make perfect contact. The result shows that nano PCM assisted  $T_{\text{PV}}$  reduced from 68.46 °C to 36.04 °C with the help of nanofluid.

Modjinou et al. comparatively analyzed macro encapsulated PCM, micro-channel heat pipe (MCHP), and regular PVT with water [28]. They found that PVT-PCM and PVT-MCHP enhanced both electrical and thermal performance. Notably, PCM-based PV module maintains constant temperature whenever there is a sudden drop in ambient temperature. Acetone influenced MHCP gains higher performance than regular PVT setup since refrigerant fluid leads to enhance the heat transfer.

PCM-only (passive cooling) incorporated PV modules are widely performed to enhance electrical efficiency without using an external source, and this system is totally autonomous and maintenance-free. Sandro et al. examined RT 38 and pork fat as a PCM in Croatia. Both PCM performed well throughout the year and there was no noticeable difference in  $T_{\text{PV}}$  reduction except in

June when ambient temperature is higher [29]. Zhao et al. analyzed different melting temperatures of PCM (PCM15, PCM20, PCM25, and PCM30) using MATLAB to find the role of PCM melting temperature [30]. A higher melting range of PCM sustains a longer time in summer, and a lower melting range of PCM performs well in winter (PCM20). This study enhanced by 2.4% the annual electric energy production.

The orientation of the PV module along with PCM plays an energetic role in  $T_{PV}$  reduction because, internally, PCM gains thermal energy by both the conduction and the convection [31]. When the PV-PCM tilt increases, PCM internal convection also increases and it helps to reduce the higher  $T_{PV}$ . During PCM melting, thermal energy gains by convection and it activates latent heat property, and conduction occurs during PCM solid state. Thermal variation on the PV module was simulated using ANSYS fluent under different climatic conditions such as 1–5 m/s wind variation. It showed an increase in wind speed and wind azimuth angle lead to dissipate higher thermal energy from both the PV module and the PCM container, which encourages heat transfer between the PV module and the PCM. A 22.6 °C melting range of PCM extracts higher heat than a 30.6 °C melting range of PCM [32].

In the passive cooling system, PCM temperature has been dissipated naturally without using any working fluid. Mostly, PCM filled in a container that is made up of high thermal conducting material. Considering cost-effectiveness and high thermal conductivity, aluminium is more widely used as a PCM container than nickel, stainless steel, and iron. Thin aluminium is difficult to weld because of its melting temperature, which is lower than other metals. During sunny days, PCM changes its phase and, considering this phase change, PCM container is fabricated in the thickness of 4–8 mm metal [32–36]. In  $T_{PV}$  reduction, low operating PCM temperature is used, which is sensitive in thermal conduction whenever the thickness of PCM container material increases. To facilitate thermal dissipation, the high conducting heatsink has been attached behind the PCM container.

Rajvikram et al. conducted a comparative analysis of PV with heatsink, PCM, and PCM–heatsink [37]. The results show that PV only and heatsink-assisted PV module maintain 1 °C reduction. PCM integrated PV module regulates better  $T_{PV}$  than heatsink by almost 7.7 °C because PCM enables high heat transfer from PV module. Finally, PCM–heatsink controls better than only heatsink or PCM, because it dissipates the stored thermal energy to the ambient during sunshine hours, which leads to maintaining a lower PCM temperature than only PCM and this discharge helps to transfer the heat from PV module and PCM.

It was noticed that using heatsink for PCM-based passive cooling technique enhances  $T_{PV}$  reduction [38]; however, the PV module backside (tedlar) is made up of non-metal, the whole PV module is fragile, and it is not advisable to keep the PCM container or PCM container with heat sink. To obtain perfect physical contact, PCM container is attached to the PV module back surface using high-temperature adhesive material or conducting oil, even though perfect physical contact is not justified. It was reported that total weight of the system could increase due to the thickness of PCM container material and fastening heatsink behind the PCM container. Attaching a PCM container or PCM container with heatsink reduces  $T_{PV}$ , but it damages the PV module's physical structure.

To prevent this contact loss and physical damage, PCM is filled on the back surface of the PV module directly [39]. Nada et al. used 10-cm PCM and its rear side was sealed using a 5-mm galvanized sheet to prevent leaks [40]. The comparative study of RT55 as pure PCM and  $Al_2O_3$  nanoparticle composited PCM shows better  $T_{PV}$  reduction and the result shows that pure PCM reduced a maximum of 8.1 °C and composite PCM reduced 10.6 °C. The reason behind the  $T_{PV}$  reduction of composite PCM is its enhanced thermal conductivity. Even though PCM is an effective thermal energy storage material, it has a lack of thermal conductivity. This low thermal conductivity creates thermal conduction barrier within the PCM.

Stropnik et al. conducted TRNSYS simulation for Ljubljana location using 3.5-cm RT28HC and they validated it with experimental results [41]. Filling PCM directly behind the PV module enhances heat transfer because PV module back surface temperature is directly in contact with PCM and

there is no intermediate layer. The rear side of the PCM is covered by 5-mm acrylic glass, and the direct enforcement of PCM leads to reduce the  $T_{PV}$  by a maximum of 35.6 °C. The relative error of the simulation is less than 3.8% compared to the experimental results. Total energy production was enhanced from 242.36 to 260.17 kWh/year and, especially from March to September, better performance is achieved.

Hasan Mahamudul et al. conducted the performance analysis of RT 35 PCM under Malaysian climatic condition with a thickness of 2 cm, which is filled and fitted within the PV module frame height, and the rear side of PCM is closed by using fiber optic glass [42,43]. The results show that a maximum of 10–12 °C reduction is achieved, but this system yields  $T_{PV}$  reduction for only 4 h because the amount of PCM used in this system is less. Some of the literature works are summarized in Table 1 for the understanding of the PCM behavior in PV module cooling under different climatic condition. Selecting appropriate melting range of PCM is one of the most crucial decisions in PV module cooling because thermal absorption of the PCM relies on its melting range and natural factors, mainly ambient temperature, humidity, and wind speed [44].

The existing literature makes clear that PCM is an effective thermal absorber and storage medium for  $T_{PV}$  reduction. PCM only and composite PCM gains great attention because of its zero maintenance and free from external energy. Systematically, PCM stores thermal energy during sunshine hours and it discharges at night, which makes this system free from maintenance and external sources. The only drawback in this system is physical contact between the PV module and the PCM container because it could damage the physical structure of the PV module due to forging hard metal onto the soft material of the PV module. Considering contact loss and weight, filling liquid PCM behind the PV module is the most effective and safest method to reduce the  $T_{PV}$ .

The main objective of this research was to analyze the effectiveness of the direct filling PCM on the back surface (tedlar) of the PV module for the summer season. OM29 is used as PCM for the location of Madurai, India (9.88° N, 78.08° E) to regulate the excess  $T_{PV}$ . In this current work, thermal absorption and dissipation of the PCM are exclusively discussed in the following section.

**Table 1.** Literature review of PCM integrated PV module.

Author	PCM/Location	System Description	$T_{PV}$ without PCM (°C)	$T_{PV}$ with PCM (°C)
Waqas et al., [44]	RT44/PV	PCMs are filled in a movable container to detach from the PV module back surface when it turns to be liquid. Yearly experimental results reveal that in summer there occurred a higher $T_{PV}$ reduction.	64	42
Hasan et al., [45]	RT42/PV	Yearly performance of RT42 integrated PV module enhances the electrical efficiency by about 5.9% and higher $T_{PV}$ reduction was achieved during April.	71	61
Zhenpeng et al., [46]	Paraffin 35/China	One month experimental analysis shows that, on 19 July, the highest electrical energy conversion noticed in the range of 499–524 Wh.	68.7	53
Leila et al., [47]	Sheep fat/indoor	Sheep fat as PCM performed better than paraffin wax and cooled water flows in the channel to enhance the heat transfer.	87	61.5

Table 1. Cont.

Author	PCM/Location	System Description	T <sub>PV</sub> without PCM (°C)	T <sub>PV</sub> with PCM (°C)
Nasrin et al., [48]	Composed oil/ indoor	Zigzag PCM container along with the combination of composed oil (coconut oil+sunflower oil) with boehmite. The final result aids in better T <sub>PV</sub> reduction for composed oil with boehmite.	72	42.5
Sajan et al., [49]	RT30/ India	Hybrid application of water-based PCM integration enhances the efficiency more than water-based cooling technique.	78	57
Nada et al., [40]	RT55/ Egypt	Al <sub>2</sub> O <sub>3</sub> nanoparticle improves the PCM thermal absorption capability with an increase in thermal conductivity.	75	49.3
Dianhong et al., [50]	Paraffin 50/China	The thermoelectric generator attached heatsink incorporated behind the PCM container to utilize the stored thermal energy of PCM.	65	51
Torsten et al., [51]	RT54HC/ Qatar	Metal fiber porous foam is impregnated with PCM to enhance the higher heat transfer from the PV module to PCM.	80	60
Ankita et al., [52]	OM39/ France	A fully wetted absorber channel removes the thermal energy from the PV module and it transfers to the PCM container.	69.17	53.86
Sardarabadu et al., [53]	Paraffin 42/Iran	Deionized water and ZnO nanofluid used as working fluid to carry out the PCM temperature for PVT application.	62	45
Modjinou et al., [28]	PCM 45/ China	A microchannel heat pipe is used to circulate the working fluid for both PVT and PVT- PCM.	75	60
Soares et al., [54]	RT22/ Portugal	Five days of experimental results reveal that movable thermal energy storage system claims negative impact on peak sunshine hours because selected RT22 PCM is not capable of this desired location.	58	72

## 2. Materials and Methods

### 2.1. Phase Change Material

OM29 is a commercial organic PCM purchased from Pluss [43], India, and it is a combination of several fatty acids. The physical appearance of OM29 is a white wax at 25 °C (solid-state). OM29 was tested by PLUSS T-History method, resulting in 29 °C onsets melting temperature with high latent heat of fusion, which makes this PCM able to store thermal energy effectively. In addition, OM29 is chemically and thermally stable for 2000 cycles, which means OM29 can perform effectively for 2000 days. It is considered that every single day T<sub>PV</sub> reduction is equivalent to a single thermal cycle. The experimental location is rich in strong sunshine of approximately 300 days per year, which means OM29 can perform effectively for 6.5 years without degrading its thermal property and performance. The thermophysical properties of OM29 are listed in Table 2.

**Table 2.** Thermophysical properties of PCM [43].

Sl.	Property	Range
1	Melting temperature (°C)	29
2	Freezing temperature (°C)	26
3	Latent heat of fusion (kJ/kg)	194
4	Liquid density (Kg/m <sup>3</sup> )	870
5	Solid density (Kg/m <sup>3</sup> )	976
6	Liquid specific heat capacity (kJ/kgK)	2.71
7	Solid specific heat capacity (kJ/kgK)	2.32
8	Liquid thermal conductivity (W/mK)	0.172
9	Solid thermal conductivity (W/mK)	0.293
10	Congruent melting	YES
11	Thermal stability (No.)	~2000
12	Maximum operating temperature	120

## 2.2. Experimental Setup

Two identical 20 Wp polycrystalline PV modules (Loom solar with the dimension 450 mm × 350 mm × 22 mm) were used in this experiment, one for PV without PCM and another for PV with PCM, as shown in Figure 1. Without further processing, 2.8 kilograms of liquid OM29 PCM was filled on the backside of the PV module with 5% space left for volume change during phase transition or volume expansion. Over the PCM layer, the rear side of the PCM was enclosed by using a 0.5-mm tin combined with aluminium sheet and, thus, leakages were protected during phase change.



**Figure 1.** Experimental setup for PV with and without PCM using OM29.

The experiment was conducted in summer (6 July 2019) at the location of 9.88 N, 78.08 E. To make an effective comparison of OM29, which was incorporated for the PV module cooling, the front and back surface of the PV module temperature was captured using FLIR thermal imaging camera every 30 min for PV without PCM. For the PV with PCM front surface was captured, but it was difficult to capture the back surface of the PV module because PV module back surface was not exposed to the camera as it was incorporated with the PCM. Thus, PCM back sheet temperature was captured to analyze the thermal dissipation of the PCM.

## 3. Thermal Heat Transfer Model

### 3.1. Heat Transfer Model for PV without PCM

Conventional PV module thermal characteristics are represented in the form of a heat transfer model, as shown in Figure 2. In the conventional system, the PV module generated thermal energies and they are mostly dissipated to the surrounding, depending on the ambient temperature ( $T_{amb}$ ) and wind speed.

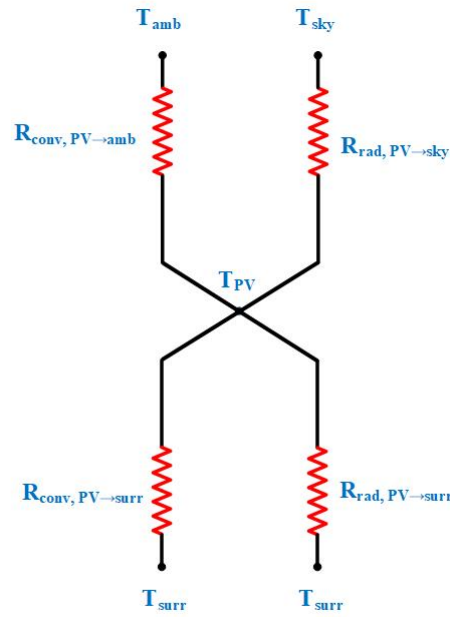


**Figure 2.** Heat transfer model for PV without PCM.

In hot region, less thermal dissipation occurs because of high  $T_{amb}$  and low wind speed, which increases the  $T_{PV}$  because excess thermal energy has been dissipated by radiation ( $R_{rad, PV \rightarrow sky}$  and  $R_{rad, PV \rightarrow surr}$ ) and natural convection ( $R_{conv, PV \rightarrow amb}$  and  $R_{conv, PV \rightarrow surr}$ ) on both the top and the bottom surface of the PV module.

Thermal energy dissipations are exclusively represented in the form of an energy balance equation in the following subsection.

### 3.1.1. Energy Balance for PV without PCM

The solar PV module is a specific heat storage material, and it stores thermal energy during the photovoltaic effect. Equation (2) denotes the total amount of thermal energy stored in the PV module corresponding to the solar irradiance, which is absorbed and transmitted to the solar cell for the energy conversion process, and during that time the PV module generates thermal energy. That energy is transferred to the ambient and sky by the mode of convection and radiation over the flat surface of the PV module, respectively. The rear side of the PV module transfers thermal energy to the surrounding by natural convection and radiation. PV module electrical efficiency is directly correlated with the  $T_{PV}$ .

$$m_{PV}C_{PV}\frac{dT_{PV}}{dt} = [\alpha_g\tau_g I(t) - h_{conv,g \rightarrow amb}(T_{PV,g} - T_{amb}) - h_{rad,g \rightarrow sky}(T_{PV,g} - T_{sky}) - h_{conv,t \rightarrow surr}(T_{PV,t} - T_{surr}) - h_{rad,t \rightarrow surr}(T_{PV,t} - T_{surr}) - \eta_{PV}I(t)]\beta A_{PV} \quad (2)$$

where  $m_{PV}$  is the weight of the PV module;  $C_{PV}$  is the specific heat capacity of the PV module;  $\alpha_g$  is the absorbance of the PV module glass;  $\tau_g$  is the transmittance of the PV module;  $I$  is the solar irradiance in  $W/m^2$ ;  $t$  is the time in s;  $h_{conv,g \rightarrow amb}$  is the convection heat transfer between PV module glass and ambient ( $W/m^2\text{ }^\circ C$ );  $h_{rad,g \rightarrow sky}$  is the radiation heat transfer between PV module glass and sky ( $W/m^2\text{ }^\circ C$ );  $h_{conv,t \rightarrow surr}$  is the convection heat transfer between PV module tedlar and surrounding ( $W/m^2\text{ }^\circ C$ );  $h_{rad,t \rightarrow surr}$  is the radiation heat transfer between PV module tedlar and surrounding ( $W/m^2\text{ }^\circ C$ );  $T_{PV,g}$  is the PV module glass temperature in  $^\circ C$ ;  $T_{amb}$  is the ambient temperature in  $^\circ C$ ;  $T_{sky}$  is the sky temperature in  $^\circ C$ ;  $T_{PV,t}$  is the PV module tedlar temperature in  $^\circ C$ ;  $T_{surr}$  is the surrounding temperature in  $^\circ C$ ;  $\eta_{PV}$  is the efficiency of the PV module in %;  $\beta$  is the packing factor; and  $A_{PV}$  is the area of the PV module.

Convection over the PV module majorly occurs with the influence of wind ( $v$ ) and an increase in wind speed over the surface of the PV module dissipates higher thermal energy to the ambient, as represented by Equation (3).

$$h_{\text{conv,g} \rightarrow \text{amb}} = 2.8 + 3v, 0 < v < 7\text{m/s} \quad (3)$$

PV module front surface radiates thermal energy to the sky and this radiation truly depends on the emissivity of the solar PV module glass [55]. It is represented by Equation (4).

$$h_{\text{rad,g} \rightarrow \text{sky}} = \epsilon_g \sigma (T_{\text{PV,g}} + T_{\text{sky}}) (T_{\text{PV,g}} + T_{\text{sky}})^2 \quad (4)$$

where  $\sigma$  is the Stefan–Boltzmann constant and  $\epsilon_g$  is the emissivity of the PV module glass.

Long-range thermal radiation to the sky is calculated using Equation (5) [56],

$$T_{\text{sky}} = 0.0522 * T_{\text{amb}}^{0.5} \quad (5)$$

The backside of the PV module dissipates thermal energy to the surroundings. Usually, this convection is poor due to the thermal resistance. PV module dissipated thermal energy stagnates in the area between the PV module backsurface and the ground. Especially the hot and low wind area suffers in thermal stagnation. This stagnation leads to reduce the thermal conductivity of air because convection depends on the surrounding air thermal conductivity, as expressed in Equation (6), and the increase in air temperature causes to reduce the thermal conductivity of the air.

$$h_{\text{conv,t} \rightarrow \text{surr}} = \frac{K_{\text{air}}}{L_{\text{PV}}} \text{Nu}_{\text{air}} \quad (6)$$

where  $K_{\text{air}}$  is the thermal conductivity of air;  $L_{\text{PV}}$  is the PV module length; and  $\text{Nu}_{\text{air}}$  is Nusslets Number.

The rear side of the PV module Nusselt number is calculated using Equation (7) and radiation to the surrounding using Equation (8).

$$\text{Nu}_{\text{air}} = \left\{ 0.825 + \frac{0.387R_a^{1/6}}{\left[ 1 + \left( \frac{0.492}{\text{Pr}} \right)^{9/6} \right]^{8/27}} \right\}^2 \quad (7)$$

where  $R_a$  is the Rayleigh number;  $\text{Pr}$  is the Prandtl number; and  $\epsilon_t$  is the Emissivity of the PV module tedlar.

$$h_{\text{rad,t} \rightarrow \text{surr}} = \epsilon_t \sigma (T_{\text{PV,t}} + T_{\text{surr}}) (T_{\text{PV,t}} + T_{\text{surr}})^2 \quad (8)$$

Electrical efficiency of the PV module is calculated using Equation (9) [57],

$$\eta_{\text{PV}} = \eta_{\text{STC}} [1 - \beta_{\text{STC}} (T_{\text{PV}} - T_{\text{STC}})] \quad (9)$$

where  $\eta_{\text{PV}}$  is the Efficiency of the PV module in %;  $\eta_{\text{STC}}$  is the PV module efficiency at standard test condition in %;  $T_{\text{PV}}$  is the PV module temperature in °C;  $T_{\text{STC}}$  is the Standard test condition temperature in °C; and  $\beta_{\text{STC}}$  is the Temperature Coefficient.

### 3.2. Heat Transfer Model for PV with PCM

Excess thermal energy from the PV module is absorbed by PCM, which is filled up on the back surface. The conventional PV module rear surface dissipates thermal energy to the surrounding with the help of temperature difference and wind. In this model, PCM plays a major role during energy conversion time by absorbing the excess thermal energy and, simultaneously, it is expected to

discharge. The rear surface of the PV module thermal energy is transferred to the PCM by conduction ( $R_{\text{cond, PV} \rightarrow \text{PCM}}$ ) and it is stored in it. Stored PCM thermal energy is transferred to the PCM back-sheet by conduction ( $R_{\text{cond, PCM} \rightarrow \text{Al}}$ ). From PCM back sheet, thermal energy is dissipated to the surrounding by natural convection ( $R_{\text{conv, Al} \rightarrow \text{surr}}$ ) and radiation ( $R_{\text{rad, Al} \rightarrow \text{surr}}$ ). Default front side of the PV module dissipates thermal energy by convection ( $R_{\text{conv, PV} \rightarrow \text{amb}}$ ) and radiation ( $R_{\text{rad, PV} \rightarrow \text{sky}}$ ). The working principle of the PCM integrated PV module is represented in the form of a heat transfer model, as shown in Figure 3.

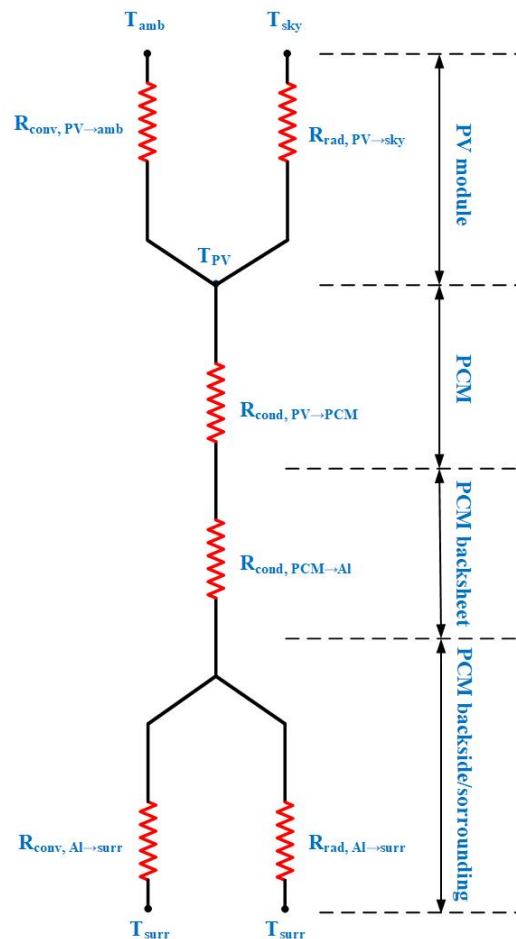


**Figure 3.** Heat transfer model for PV with PCM.  $R_{\text{conv, PV} \rightarrow \text{amb}}$  is the convection resistance between the PV front side and ambient;  $R_{\text{rad, PV} \rightarrow \text{sky}}$  is the radiation resistance between the PV front side PV and sky;  $R_{\text{conv, PV} \rightarrow \text{surr}}$  is the convection resistance between the PV rear side and ambient;  $R_{\text{rad, PV} \rightarrow \text{surr}}$  is the radiation resistance between the PV rear side and surrounding;  $R_{\text{cond, PV} \rightarrow \text{PCM}}$  is the conduction resistance between the PV rear side and PCM;  $R_{\text{cond, PCM} \rightarrow \text{Al}}$  is the conduction resistance between the PCM rear side and PCM back sheet;  $R_{\text{conv, Al} \rightarrow \text{surr}}$  is the convection resistance between the rear side of the PCM back sheet and surrounding; and  $R_{\text{rad, Al} \rightarrow \text{surr}}$  is the radiation resistance between the rear side of the PCM back sheet and surrounding.

### 3.2.1. Energy Balance for PCM Integrated PV Module

Equation (10) denotes the amount of thermal energy stored in the PV module after PCM absorption. The front side of the PV module absorbs and transmits the solar irradiance to the PV module for energy conversion. During that time, the PV module generates thermal energy, and it is absorbed by the PCM, which is incorporated on the back surface by direct conduction. The rest is dissipated to the sky and the ambient the same as for PV without PCM. In this case, the electrical efficiency of the PV module is directly correlated with the amount of thermal energy absorbed by PCM.

$$m_{PV}C_{PV}\frac{dT_{PV}}{dt} = [\alpha_g\tau_g I(t) - h_{conv,g\rightarrow amb}(T_{PV,g} - T_{amb}) - h_{rad,g\rightarrow sky}(T_{PV,g} - T_{sky}) - h_{cond,t\rightarrow PCM}(T_{PV,t} - T_{PCM}) - \eta_{PV}I(t)]\beta A_{PV} \quad (10)$$

where  $h_{cond,t\rightarrow PCM}$  is the conduction heat transfer between PV module tedlar and PCM ( $W/m^2\text{ }^\circ\text{C}$ ) and  $T_{PCM}$  is the PCM temperature in  $^\circ\text{C}$ .

Moreover, regulating  $T_{PV}$  for longer and effectively depends on the ratio of PCM thermal conductivity and PCM thickness, as expressed in Equation (11).

$$h_{cond,t\rightarrow PCM} = \frac{K_{PCM}}{\Delta X_{PCM}} \quad (11)$$

where  $K_{PCM}$  is the PCM thermal conductivity and  $\Delta X_{PCM}$  is the PCM thickness.

### 3.3. Energy Balance for Conduction Sourced PCM

Equation (12) denotes the amount of thermal energy stored in the PCM during energy conversion. Excess thermal energy from the PV module is transferred to the PCM by conduction and this energy is stored in three different phases, as expressed in Equation (13). During charging and off sunshine hours, PCM thermal energy is transferred to the PCM back sheet by conduction. Thus, dissipating PCM thermal energy to the surrounding leads to enhance the heat transfer from the PV module to PCM. PCM back sheet transfers thermal energy to the surrounding by natural convection and radiation because the PCM backside is not insulated. PCM should discharge the stored thermal energy before the next sunshine (overnight), else the next day PCM would not be able to initiate the absorption effectively.

$$m_{PCM}C_{PCM}\frac{dT_{PCM}}{dt} = [-h_{cond,t\rightarrow PCM}(T_{PV,t} - T_{PCM}) - h_{cond,PCM\rightarrow Al}(T_{PCM} - T_{Al}) - h_{conv,Al\rightarrow surr}(T_{Al} - T_{surr}) - h_{rad,Al\rightarrow surr}(T_{Al} - T_{surr})]\beta A_{PCM} \quad (12)$$

where  $m_{PCM}$  is the mass of PCM;  $C_{PCM}$  is the storage capacity of PCM;  $h_{cond,PCM\rightarrow Al}$  is the conduction heat transfer between PCM and PCM back sheet ( $W/m^2\text{ }^\circ\text{C}$ );  $h_{conv,Al\rightarrow surr}$  is the convection heat transfer between PCM back sheet and surrounding ( $W/m^2\text{ }^\circ\text{C}$ );  $h_{rad,Al\rightarrow surr}$  is the radiation heat transfer between PCM back sheet and surrounding ( $W/m^2\text{ }^\circ\text{C}$ );  $T_{PCM}$  is the PCM temperature ( $^\circ\text{C}$ );  $T_{Al}$  is the PCM back sheet temperature ( $^\circ\text{C}$ ); and  $T_{surr}$  is the surrounding temperature ( $^\circ\text{C}$ ).

Equation (13) represents three different phases of PCM during thermal energy storage. When the PCM temperature is less than the melting point, thermal energy stores in the form of solid specific heat capacity. When it is equal to the melting point, PCM stores thermal energy in the form of latent heat of fusion. It is recommended to maintain the PCM to be in latent heat of fusion state because the liquid specific heat capacity of the PCM is not effective in storing thermal energy and thus thermal conductivity of the liquid PCM is low.

$$C_{PCM} = \begin{cases} \text{solid specific heat capacity, } T_{PCM} < T_{melt} \\ \text{latent heat of fusion, } T_{PCM} = T_{melt} \\ \text{liquid specific heat capacity, } T_{PCM} > T_{melt} \end{cases} \quad (13)$$

where  $T_{melt}$  is the melting temperature.

## 4. Results and Discussions

### 4.1. Temperature Profile of PV Module

The experimental setup of the PV with and without PCM was developed and examined in the summer (6 July 2019) under the direct sunlight to observe the thermal behavior. During every 30 min interval, thermal images of the PV module and PCM back sheet were taken. Figures 4 and 5

show the meteorological data of solar irradiance and ambient temperature on the corresponding experimental day.

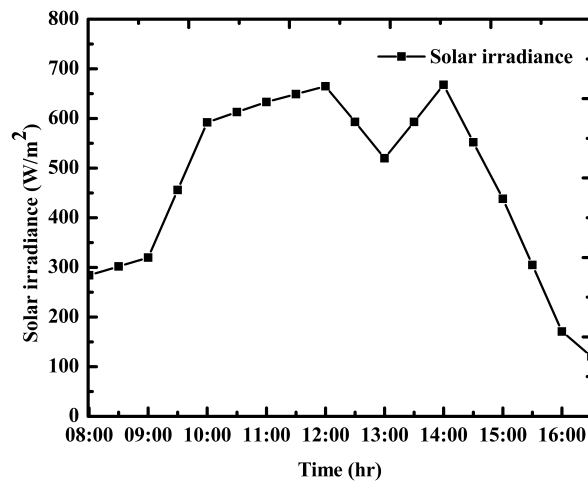


Figure 4. Experimental day solar irradiance.

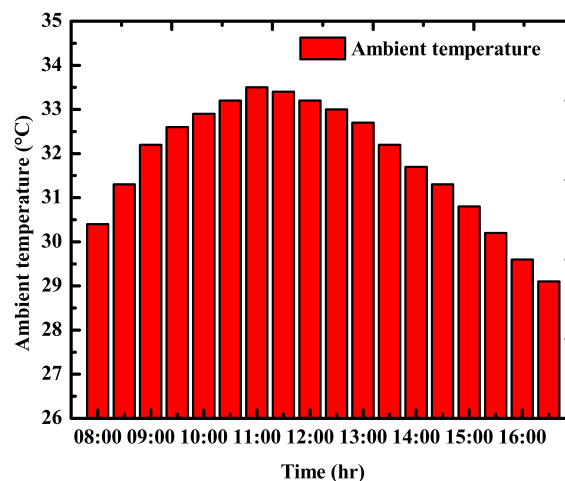
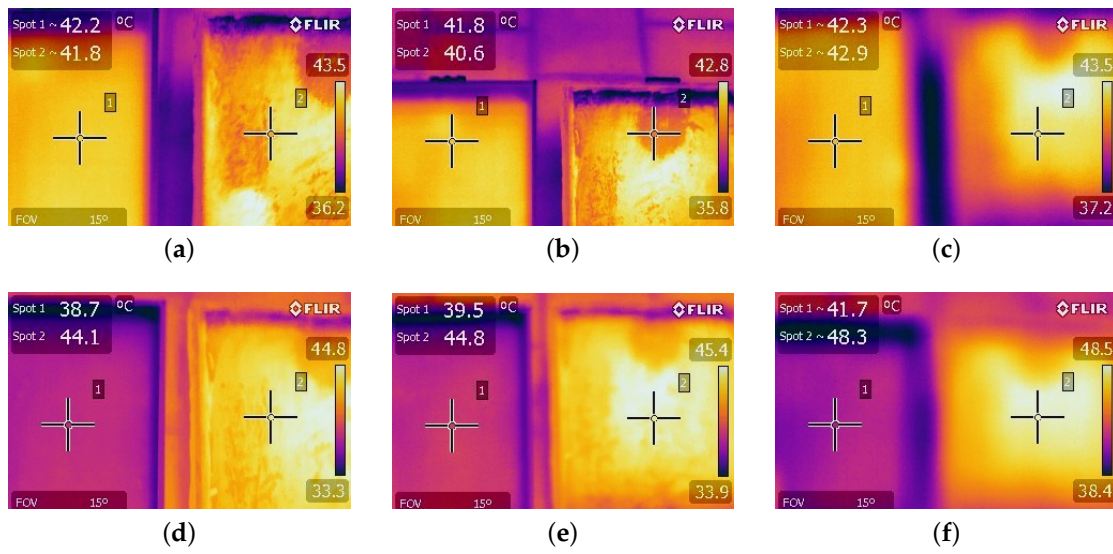


Figure 5. Experimental day ambient temperature.

The examined OM29 organic PCM enabled thermal energy transfer from PV module to PCM by conduction. Figure 6a shows a thermal image of the PV module at 8:00. There was a noticeable  $T_{PV}$  reduction of  $0.4\text{ }^{\circ}\text{C}$  because, during that time, PCM had solid specific heat capacity as well semi mushy region.

PCM absorbed the  $T_{PV}$  effectively when the PCM attained its melting point. The results show that PCM utilized its thermal absorbing and storing capability until 8:30 because  $T_{PV}$  reduction achieved up to 8:30 maximum of  $1.2\text{ }^{\circ}\text{C}$ . From 9:00,  $T_{PV}$  started to rise slightly less than the PV without PCM, as shown in Figure 6b,c. Even though the latent heat capacity of the PCM was high,  $T_{PV}$  reduction sustained for a lower period due to its low melting point, which is inappropriate for the selected location for the summer season. Further following this,  $T_{PV}$  was not achieved during the peak sunshine hours, as shown in Figures 7 and 8. After 9:00, PCM was completely liquid completely, as listed in Table 3. Liquid specific heat capacity was not effective for storing the thermal energy such as latent heat of fusion (mushy state).



**Figure 6.** Thermal imaging of PV module spot 1 without PCM and spot 2 with PCM: (a) 8:00; (b) 8:30; (c) 9:00; (d) 9:30; (e) 10:00; and (f) 10:30.

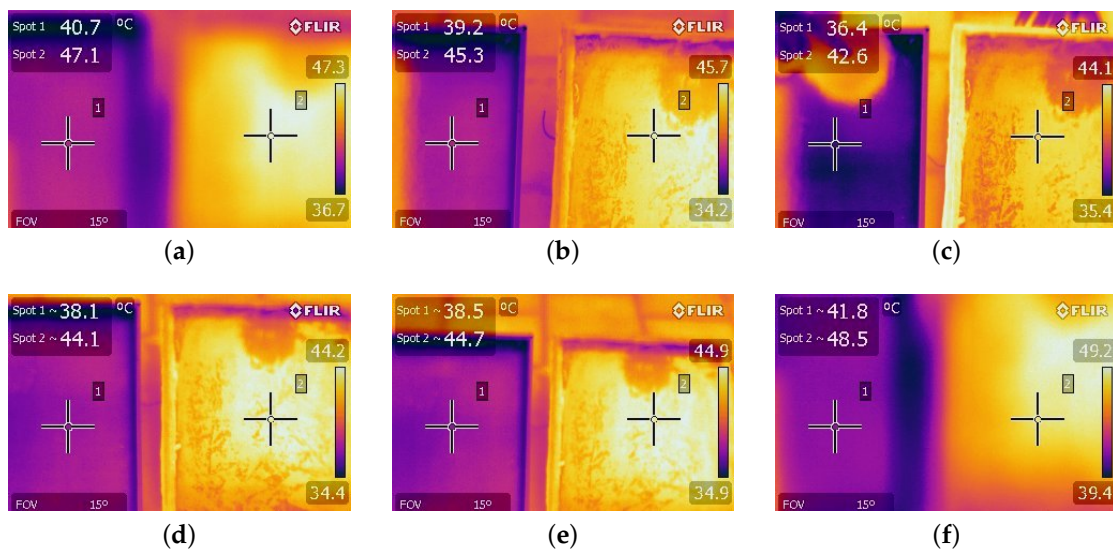


**Figure 7.** Thermal imaging of PV module spot 1 without PCM and spot 2 with PCM: (a) 11:00; (b) 11:30; (c) 12:00; (d) 12:30; (e) 13:00; and (f) 13:30.

**Table 3.** Temperature profile of PV only and PV with PCM.

Time (h)	PV without PCM ( °C)		PV with PCM ( °C)	
	Front Surface	Back Surface	PV Front Surface	PCM Backsheet
8:00	42.2	44.3	41.8	27.3
8:30	41.8	43.8	40.6	28.1
9:00	42.3	44.6	42.9	28.9
9:30	38.7	43.6	44.1	32.5
10:00	39.5	44.1	44.8	33.8
10:30	41.7	46.8	48.3	37.5
11:00	40.7	46.1	47.1	38.6
11:30	39.2	45.8	45.3	39.1
12:00	36.4	42.8	42.6	38.4
12:30	38.1	44.5	44.1	38.7
13:00	38.5	45.3	44.7	39.1
13:30	41.8	47.1	48.5	41.9
14:00	41.6	47.9	48.5	41.6
14:30	41	47.2	47.7	41.3
15:00	41.2	46.9	47.9	40.9
15:30	41.5	47.1	48.1	41.5
16:00	40.6	46.8	47.2	41.1
16:30	39.3	46.4	45.4	40.9

Secondly, in this experiment, PCM failed to discharge the stored thermal energy during sunshine hours, because thermal conductivity of the PCM was low, increasing the thermal conduction resistance within the liquid PCM, and the PCM back sheet (tin combined with aluminium) was not an effective thermal dissipater as compared to pure aluminium [39]. Increasing the thickness of PCM enhanced the heat transfer between the PV module and the PCM [58–60]. In this system, 2-cm PCM was used, which melted completely within 1 h from and, during the rest of the period,  $T_{PV}$  increased to a maximum of 7 °C, which was more than the conventional PV module (PV without PCM), as shown in Figures 8 and 9.

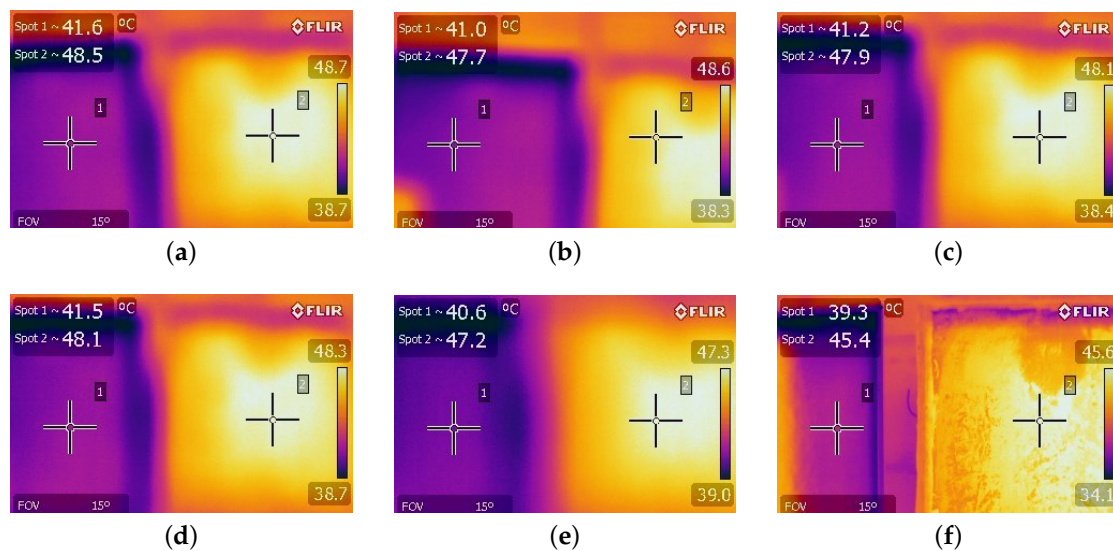


**Figure 8.** Thermal imaging of PV module spot 1 without PCM and spot 2 with PCM: (a) 14:00; (b) 14:30; (c) 15:00; (d) 15:30; (e) 16:00; and (f) 16:30.

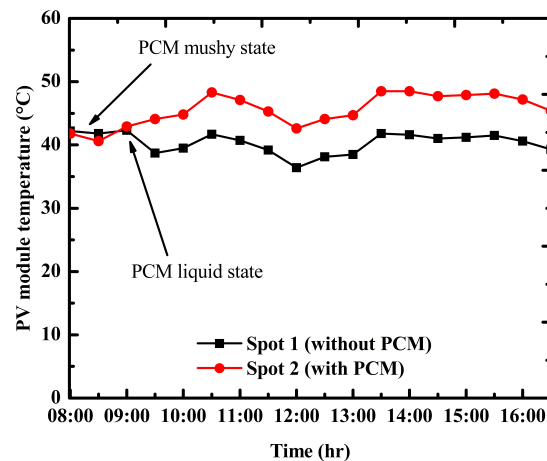


Figure 9. Overall PV module temperature with and without PCM.

The reason behind this  $T_{PV}$  rise is that the PCM integrated PV module back surface was not interacting with the ambient and wind. Since PCM was filled on the back surface of the PV module, the PCM integrated PV module thermal dissipation depended on the PCM and PCM container material. For PV without PCM, thermal energy could be easily dissipated to the surrounding because there was no storage medium between the PV module back surface and the surrounding. However, PCM integration reduced  $T_{PV}$  effectively when the PCM sustained the mushy state for a longer time, but, once it became liquid, PCM acted as an insulating material compared to PV without PCM. Thus, PV without PCM had a lower  $T_{PV}$  than PV with PCM. Since the back surface of the PV module had PCM, it had stored thermal energy in it. Note that the experimental day ambient temperature was higher than the PCM melting temperature.

The 2.2-cm PCM layer contained only 2.8 kilograms of PCM. It could not maintain the mushy state for a long time and had difficulty reducing the PCM temperature lower than the melting temperature using passive cooling because it depended on the natural factor. If the PCM back sheet also had a good thermal dissipating material, PCM would not reach its melting point or mushy state again during the experimental day, because ambient temperature was higher than the PCM melting point. Thus, the only possible way is active cooling method, which could lower the PCM temperature forcibly and help to maintain the mushy state for longer time. Many researchers addressed this ineffective  $T_{PV}$  reduction by categorizing inappropriate PCM melting temperature selection [44], PCM thickness [61], and PCM thermal conduction barrier [35]. Existing experimental investigation states that PCM selection is the crucial term in the whole process of the PV module cooling; selecting a lower or higher melting range of PCM will make the  $T_{PV}$  reduction ineffective because  $T_{PV}$  reduction is only achieved when the PCM reaches its melting point. Lower melting range of PCM will utilize its latent heat property before the peak sunshine hours and higher melting range of PCM will not use its latent heat property during peak sunshine hours. The only solution for this issue is to select PCM with melting range 2–3 °C higher than the peak ambient temperature so that the PCM will not gain thermal energy from ambient during sunshine hours.

During the experimental day, the recorded high ambient temperature was 33.5 °C. If the selected PCM melting range were 35–36 °C, a better  $T_{PV}$  reduction would have been achieved. A general rule of thumb indicates that an increase in the thickness of PCM leads to sustainability of the  $T_{PV}$  reduction for longer time, as well as creates the thermal conduction barrier during thermal absorption. To overcome this issue, several researchers have incorporated thermal additives to enhance the thermal conductivity of the PCM by adding metal foam [62], metal scrap [63], copper powder [64], graphite [64], expandable graphite [65], and nanoparticles [48].

#### 4.2. Temperature Corrected Electrical Efficiency

The electrical efficiency of the PV module was directly correlated with the  $T_{PV}$ ; the increase in  $T_{PV}$  led to reduce electrical efficiency by  $-0.43\%/^{\circ}\text{C}$ . However, this experiment enhanced the electrical efficiency until 8:30; afterwards, PCM integrated PV module electrical efficiency was lower than PV without PCM, as shown in Figure 10.

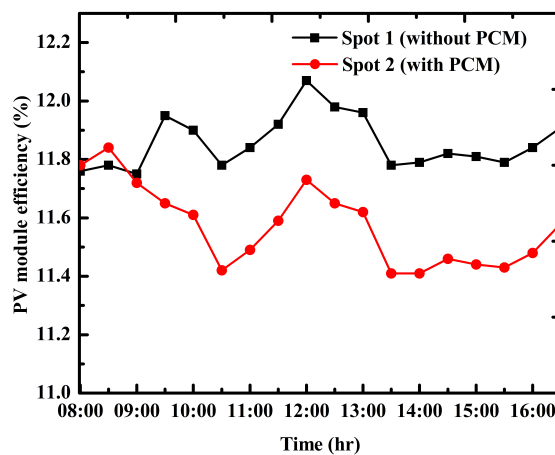


**Figure 10.** Temperature corrected electrical efficiency of the PV module with and without PCM.

The corresponding increase in  $T_{PV}$  in the PCM integrated PV module reduced the electrical efficiency by a maximum of 0.38%, which shows that PCM acted as a thermal source to the PV module when it turned completely liquid.

#### 5. Conclusions

The heat transfer capability from the PV module to the PCM can be greatly enhanced by the direct filling of PCM behind the PV panel without the use of an intermediate layer. It is an efficient way of keeping the temperature of the PV panel within a reasonable limit by means of passive cooling methodology. However, if an OM29 PCM tends to behave differently in the summer season because of the atmospheric condition. On the day of experimentation,  $T_{PV}$  dropped up to 8:30; after that, the OM29 was unable to absorb the PV module generated thermal energy due to the impact of a lower melting range of the PCM. The experimental results reveal that the OM29 PCM was not capable of PV module cooling, especially for a hot and humid region such as India. Many researchers addressed this issue because selecting PCM melting temperature is the most challenging task for the module cooling for an entire year. The selected OM29 PCM performed well in winter, while, in summer, it did not dissipate the stored thermal energy; in addition, OM29 lost its latent heat property within 8:30 and after that PCM started to act as an insulating material for the PV module. Hence, it was concluded that OM29 was not a suitable PCM for cooling the PV module in the summer season. Further, it is recommended to select an appropriate PCM for this desired location. In addition, it is necessary to increase the thickness of the PCM and thermal conductivity in order to attain better absorption and dissipation.

**Author Contributions:** R.M.E. and K.V. carried out the experimental research, analysis of results and writing the draft of the manuscript. A.R.K. carried out the proofreading and formatting of the research work and paper writing. U.S. and D.A. carried out the proof reading of the manuscript and funding the publication of the manuscript. All authors have read and agreed to the published version of the manuscript.

**Funding:** The APC was funded by the College of Engineering, Prince Sultan University, Riyadh-11586, Saudi Arabia.

**Conflicts of Interest:** The authors declare no conflict of interest.

## References

1. Zedalis, R.J. *Global Energy & CO2 Status Report*; Technical Report; Routledge: London, UK, 2017. [\[CrossRef\]](#)
2. Qazi, A.; Hussain, F.; Rahim, N.A.; Hardaker, G.; Alghazzawi, D.; Shaban, K.; Haruna, K. Towards Sustainable Energy: A Systematic Review of Renewable Energy Sources, Technologies, and Public Opinions. *IEEE Access* **2019**, *7*, 63837–63851. [\[CrossRef\]](#)
3. Elavarasan, R.M. Comprehensive Review on India's Growth in Renewable Energy Technologies in Comparison With Other Prominent Renewable Energy Based Countries. *J. Sol. Energy Eng.* **2020**, *142*, 1–11. [\[CrossRef\]](#)
4. Elavarasan, R.M.; Shafiullah, G.M.; Kumar, N.M.; Padmanaban, S. A State-of-the-Art Review on the Drive of Renewables in Gujarat, State of India: Present Situation, Barriers and Future Initiatives. *Energies* **2020**, *13*, 40. [\[CrossRef\]](#)
5. Elavarasan, R.M. The Motivation for Renewable Energy and its Comparison with Other Energy Sources: A Review. *Eur. J. Sustain. Dev. Res.* **2019**, *3*, 1–19. [\[CrossRef\]](#)
6. Das, N.K.; Islam, S.M. Conversion Efficiency Improvement in GaAs Solar Cells. In *Large Scale Renewable Power Generation. Green Energy and Technology*; Springer: Singapore, 2014; pp. 53–75. [\[CrossRef\]](#)
7. Das, N.; Wongsodihardjo, H.; Islam, S. Modeling of multi-junction photovoltaic cell using MATLAB/Simulink to improve the conversion efficiency. *Renew. Energy* **2015**, *74*, 917–924. [\[CrossRef\]](#)
8. Subramaniam, U.; Ganesan, S.; Bhaskar, M.S.; Padmanaban, S.; Blaabjerg, F.; Almakhles, D.J. Investigations of AC Microgrid Energy Management Systems Using Distributed Energy Resources and Plug-in Electric Vehicles. *Energies* **2019**, *12*, 2834. [\[CrossRef\]](#)
9. Kumar, A.R.; Thangavelusamy, D.; Padmanaban, S.; Kothari, D.P. A Modified PWM Scheme to improve AC Power Quality for MLIs using PV Source. *Int. J. Power Energy Syst.* **2019**, *39*, 34–41. [\[CrossRef\]](#)
10. Sridhar, V.; Umashankar, S.; Sanjeevikumar, P.; Ramchandaramurthy, V.K.; Mihet-Popa, L.; Fedák, V. Control Architecture for Cascaded H-Bridge Inverters in Large-Scale PV Systems. *Energy Procedia* **2018**, *145*, 549–557. [\[CrossRef\]](#)
11. Elavarasan, M.; Mallick, G.; Saravanan, K. Investigations on Performance Enhancement Measures of the Bidirectional Converter in PV-Wind Interconnected Microgrid System. *Energies* **2019**, *12*, 2672. [\[CrossRef\]](#)
12. Bhukya, M.N.; Kota, V.R.; Depuru, S.R. A Simple, Efficient, and Novel Standalone Photovoltaic Inverter Configuration With Reduced Harmonic Distortion. *IEEE Access* **2019**, *7*, 43831–43845. [\[CrossRef\]](#)
13. Rajvikram, M.; Leoponraj, S. A method to attain power optimality and efficiency in solar panel. *Beni-Suef Univ. J. Basic Appl. Sci.* **2018**, *7*, 705–708. [\[CrossRef\]](#)
14. Alami, A.H. Effects of evaporative cooling on efficiency of photovoltaic modules. *Energy Convers. Manag.* **2014**, *77*, 668–679. [\[CrossRef\]](#)
15. Schiro, F.; Benato, A.; Stoppato, A.; Destro, N. Improving photovoltaics efficiency by water cooling: Modelling and experimental approach. *Energy* **2017**, *137*, 798–810. [\[CrossRef\]](#)
16. Liang, R.; Wang, P.; Zhou, C.; Pan, Q.; Riaz, A.; Zhang, J. Thermal performance study of an active solar building façade with specific PV/T hybrid modules. *Energy* **2019**, 116532. [\[CrossRef\]](#)
17. Bahaidarah, H.; Subhan, A.; Gandhidasan, P.; Rehman, S. Performance evaluation of a PV (photovoltaic) module by back surface water cooling for hot climatic conditions. *Energy* **2013**, *59*, 445–453. [\[CrossRef\]](#)
18. Sutanto, B.; Indartono, Y.S. Computational fluid dynamic (CFD) modelling of floating photovoltaic cooling system with loop thermosiphon. In Proceedings of the AIP Conference, Bali, Indonesia, 14–16 August 2019; Volume 2062, p. 020011(1-6). [\[CrossRef\]](#)
19. Sellami, R.; Amirat, M.; Mahrane, A.; Slimani, M.E.A.; Arbane, A.; Chekrouni, R. Experimental and numerical study of a PV/Thermal collector equipped with a PV-assisted air circulation system: Configuration suitable for building integration. *Energy Build.* **2019**, *190*, 216–234. [\[CrossRef\]](#)
20. Shahsavari, A.; Khanmohammadi, S.; Khaki, M.; Salmanzadeh, M. Performance assessment of an innovative exhaust air energy recovery system based on the PV/T-assisted thermal wheel. *Energy* **2018**, *162*, 682–696. [\[CrossRef\]](#)
21. Krishnan, S.; Garimella, S.; Kang, S. A novel hybrid heat sink using phase change materials for transient thermal management of electronics. *IEEE Trans. Components Packag. Technol.* **2005**, *28*, 281–289. [\[CrossRef\]](#)

22. Afshari-Bavil, M.; Dong, M.; Li, C.; Feng, S.; Zhu, L. Thermally Controllable High-Efficiency Unidirectional Coupling in a Double-Slit Structure Filled With Phase Change Material. *IEEE Photonics J.* **2019**, *11*, 1–8. [[CrossRef](#)]
23. Karthikeyan, V.; Sirisamphanwong, C.; Sukchai, S. Thermal investigation of Paraffin Wax for Low-Temperature Application. *J. Adv. Res. Dyn. Control. Syst.* **2019**, *11*, 1437–1443.
24. Stupar, A.; Drogenik, U.; Kolar, J.W. Optimization of Phase Change Material Heat Sinks for Low Duty Cycle High Peak Load Power Supplies. *IEEE Trans. Components Packag. Manuf. Technol.* **2012**, *2*, 102–115. [[CrossRef](#)]
25. Alawadhi, E. Thermal Management of Blocks in a Channel Using Phase Change Material. *IEEE Trans. Components Packag. Technol.* **2009**, *32*, 89–99. [[CrossRef](#)]
26. Fayaz, H.; Rahim, N.; Hasanuzzaman, M.; Nasrin, R.; Rivai, A. Numerical and experimental investigation of the effect of operating conditions on performance of PVT and PVT-PCM. *Renew. Energy* **2019**, *143*, 827–841. [[CrossRef](#)]
27. Al-Waeli, A.H.; Chaichan, M.T.; Sopian, K.; Kazem, H.A.; Mahood, H.B.; Khadom, A.A. Modeling and experimental validation of a PVT system using nanofluid coolant and nano-PCM. *Sol. Energy* **2019**, *177*, 178–191. [[CrossRef](#)]
28. Modjinou, M.; Ji, J.; Yuan, W.; Zhou, F.; Holliday, S.; Waqas, A.; Zhao, X. Performance comparison of encapsulated PCM PV/T, microchannel heat pipe PV/T and conventional PV/T systems. *Energy* **2019**, *166*, 1249–1266. [[CrossRef](#)]
29. Nižetić, S.; Arıcı, M.; Bilgin, F.; Grubišić-Čabo, F. Investigation of pork fat as potential novel phase change material for passive cooling applications in photovoltaics. *J. Clean. Prod.* **2018**, *170*, 1006–1016. [[CrossRef](#)]
30. Zhao, J.; Ma, T.; Li, Z.; Song, A. Year-round performance analysis of a photovoltaic panel coupled with phase change material. *Appl. Energy* **2019**, *245*, 51–64. [[CrossRef](#)]
31. Al-Jethelah, M.S.M.; Al-Sammarraie, A.; Tasnim, S.H.; Mahmud, S.; Dutta, A. Effect of convection heat transfer on thermal energy storage unit. *Open Phys.* **2018**, *16*, 861–867. [[CrossRef](#)]
32. Khanna, S.; Reddy, K.; Mallick, T.K. Performance analysis of tilted photovoltaic system integrated with phase change material under varying operating conditions. *Energy* **2017**, *133*, 887–899. [[CrossRef](#)]
33. Huang, M.; Eames, P.; Norton, B. Thermal regulation of building-integrated photovoltaics using phase change materials. *Int. J. Heat Mass Transf.* **2004**, *47*, 2715–2733. [[CrossRef](#)]
34. Nehari, T.; Benlakam, M.; Nehari, D. Effect of the Fins Length for the Passive Cooling of the Photovoltaic Panels. *Period. Polytech. Mech. Eng.* **2016**, *60*, 89–95. [[CrossRef](#)]
35. Khanna, S.; Reddy, K.; Mallick, T.K. Optimization of finned solar photovoltaic phase change material (finned pv pcm) system. *Int. J. Therm. Sci.* **2018**, *130*, 313–322. [[CrossRef](#)]
36. Biwole, P.; Eclache, P.; Kuznik, F. Improving the Performance of Solar Panels by the Use of Phase-Change Materials. In Proceedings of the World Renewable Energy Congress, Linköping, Sweden, 8–13 May 2011; Volume 57, pp. 2953–2960. [[CrossRef](#)]
37. Rajvikram, M.; Sivasankar, G. Experimental study conducted for the identification of best heat absorption and dissipation methodology in solar photovoltaic panel. *Sol. Energy* **2019**, *193*, 283–292. [[CrossRef](#)]
38. Wongwuttanasatian, T.; Sarikarin, T.; Suksri, A. Performance enhancement of a photovoltaic module by passive cooling using phase change material in a finned container heat sink. *Sol. Energy* **2020**, *195*, 47–53. [[CrossRef](#)]
39. Rajvikram, M.; Leononraj, S.; Ramkumar, S.; Akshaya, H.R.; Dheeraj, A. Experimental investigation on the abasement of operating temperature in solar photovoltaic panel using PCM and aluminium. *Sol. Energy* **2019**, *188*, 327–338. [[CrossRef](#)]
40. Nada, S.; El-Nagar, D.; Hussein, H. Improving the thermal regulation and efficiency enhancement of PCM-Integrated PV modules using nano particles. *Energy Convers. Manag.* **2018**, *166*, 735–743. [[CrossRef](#)]
41. Stropnik, R.; Stritih, U. Increasing the efficiency of PV panel with the use of PCM. *Renew. Energy* **2016**, *97*, 671–679. [[CrossRef](#)]
42. Mahamudul, H.; Silakhori, M.; Henk Metselaar, I.; Ahmad, S.; Mekhilef, S. Development of a temperature regulated photovoltaic module using phase change material for Malaysian weather condition. *Optoelectron. Adv. Mater. Rapid Commun.* **2014**, *8*, 1243–1245.
43. Polymers, P. *Technical Data Sheet of savE<sup>®</sup> OM29*; PLUSS: Haryana, India 2017.

44. Waqas, A.; Ji, J. Thermal management of conventional PV panel using PCM with movable shutters—A numerical study. *Sol. Energy* **2017**, *158*, 797–807. [[CrossRef](#)]
45. Hasan, A.; Sarwar, J.; Alnoman, H.; Abdelbaqi, S. Yearly energy performance of a photovoltaic-phase change material (PV-PCM) system in hot climate. *Sol. Energy* **2017**, *146*, 417–429. [[CrossRef](#)]
46. Li, Z.; Ma, T.; Zhao, J.; Song, A.; Cheng, Y. Experimental study and performance analysis on solar photovoltaic panel integrated with phase change material. *Energy* **2019**, *178*, 471–486. [[CrossRef](#)]
47. Siahkamari, L.; Rahimi, M.; Azimi, N.; Banibayat, M. Experimental investigation on using a novel phase change material (PCM) in micro structure photovoltaic cooling system. *Int. Commun. Heat Mass Transf.* **2019**, *100*, 60–66. [[CrossRef](#)]
48. Abdollahi, N.; Rahimi, M. Potential of water natural circulation coupled with nano-enhanced PCM for PV module cooling. *Renew. Energy* **2020**, *147*, 302–309. [[CrossRef](#)]
49. Preet, S.; Bhushan, B.; Mahajan, T. Experimental investigation of water based photovoltaic/thermal (PV/T) system with and without phase change material (PCM). *Sol. Energy* **2017**, *155*, 1104–1120. [[CrossRef](#)]
50. Li, D.; Xuan, Y.; Yin, E.; Li, Q. Conversion efficiency gain for concentrated triple-junction solar cell system through thermal management. *Renew. Energy* **2018**, *126*, 960–968. [[CrossRef](#)]
51. Klemm, T.; Hassabou, A.; Abdallah, A.; Andersen, O. Thermal energy storage with phase change materials to increase the efficiency of solar photovoltaic modules. *Energy Procedia* **2017**, *135*, 193–202. [[CrossRef](#)]
52. Gaur, A.; Ménézou, C.; Giroux-Julien, S. Numerical studies on thermal and electrical performance of a fully wetted absorber PVT collector with PCM as a storage medium. *Renew. Energy* **2017**, *109*, 168–187. [[CrossRef](#)]
53. Sardarabadi, M.; Passandideh-Fard, M.; Maghrebi, M.J.; Ghazikhani, M. Experimental study of using both ZnO/water nanofluid and phase change material (PCM) in photovoltaic thermal systems. *Sol. Energy Mater. Sol. Cells* **2017**, *161*, 62–69. [[CrossRef](#)]
54. Soares, N.; Costa, J.; Gaspar, A.; Matias, T.; Simões, P.; Durães, L. Can movable PCM-filled TES units be used to improve the performance of PV panels? Overview and experimental case-study. *Energy Build.* **2020**, *210*, 109743. [[CrossRef](#)]
55. Reiter, C.N.; Trinkl, C.; Zörner, W.; Hanby, V.I. A Dynamic Multinode Model for Component-Oriented Thermal Analysis of Flat-Plate Solar Collectors. *J. Sol. Energy* **2015**, *2015*, 1–16. [[CrossRef](#)]
56. Chaabane, M.; Mhiri, H.; Bournot, P. Thermal performance of an integrated collector storage solar water heater (ICSSWH) with phase change materials (PCM). *Energy Convers. Manag.* **2014**, *78*, 897–903. [[CrossRef](#)]
57. Skoplaki, E.; Palyvos, J. On the temperature dependence of photovoltaic module electrical performance: A review of efficiency/power correlations. *Sol. Energy* **2009**, *83*, 614–624. [[CrossRef](#)]
58. Hendricks, J.H.C.; Sark, W.G.J.H.M. Annual performance enhancement of building integrated photovoltaic modules by applying phase change materials. *Prog. Photovoltaics Res. Appl.* **2011**, *20*. [[CrossRef](#)]
59. Klugmann-Radziemska, E.; Wcisło-Kucharek, P. Photovoltaic module temperature stabilization with the use of phase change materials. *Sol. Energy* **2017**, *150*, 538–545. [[CrossRef](#)]
60. Waqas, A.; Jie, J. Effectiveness of Phase Change Material for Cooling of Photovoltaic Panel for Hot Climate. *J. Sol. Energy Eng.* **2018**, *140*, 1–19. [[CrossRef](#)]
61. Khanna, S.; Reddy, K.; Mallick, T.K. Optimization of solar photovoltaic system integrated with phase change material. *Sol. Energy* **2018**, *163*, 591–599. [[CrossRef](#)]
62. Abdulmunem, A.R. Passive Cooling By Utilizing the Combined PCM /Aluminum Foam Matrix To Improve Solar Panels Performance : Indoor Investigation. *Iraqi J. Mech. Mater. Eng.* **2017**, *17*, 712–723.
63. Maiti, S.; Banerjee, S.; Vyas, K.; Patel, P.; Ghosh, P.K. Self regulation of photovoltaic module temperature in V-trough using a metal-wax composite phase change matrix. *Sol. Energy* **2011**, *85*, 1805–1816. [[CrossRef](#)]
64. Hachem, F.; Abdulhay, B.; Ramadan, M.; El Hage, H.; El Rab, M.G.; Khaled, M. Improving the performance of photovoltaic cells using pure and combined phase change materials—Experiments and transient energy balance. *Renew. Energy* **2017**, *107*, 567–575. [[CrossRef](#)]
65. Karthikeyan, V.; Prasanna, P.; Sathishkumar, N.; Emsaeng, K.; Sukchai, S.; Sirisamphanwong, C. Selection and preparation of suitable composite phase change material for PV module cooling. *Int. J. Emerg. Technol.* **2019**, *10*, 385–394.

